Thin Cu/Ag(111) and Ag/Cu(111) structures studied with monoenergetic positrons

P. A. Huttunen* and A. Vehanen†

Laboratory of Physics, Helsinki University of Technology, 02150 Espoo, Finland
(Received 2 January 1990; revised manuscript received 9 April 1990)

The early stages of crystal growth have been studied with variable-energy positrons in conjunction with low-energy electron diffraction and Auger-electron spectroscopy. We report measurements of positron branching ratios for (0.1–10)-monolayer (ML) Cu overlayers grown on Ag(111) and for (0.1–100)-ML Ag overlayers grown on Cu(111). The results are discussed in terms of the structural and electronic properties of the surfaces as well as positron-interaction mechanisms at the surfaces. Our method is *not* sensitive to open-volume defects created during the early stages of crystal growth. Information on positron implantation at small incident energies, positron surface processes, and positron thermalization properties is extracted from experimental data.

I. INTRODUCTION

Recently there has been a lot of research activity in metallic layered structures. In particular, the early stages of crystal growth have attracted a great deal of attention (see, e.g., Ref. 1). This phase is important to many applications where surface-related properties play a major role. For example, metallic coatings may passivate the surfaces against corrosion and radiation damage, and they may result in specific optical or electrical properties or a unique catalytic activity being achieved. A myriad of different surface-sensitive techniques,[2] normally based on interactions of electrons, ions, or electromagnetic radiation with the solid, has been utilized. In the present work we report on experiments done with monoenergetic positrons on heteroepitaxial systems at low coverages.

The progress in monoenergetic positron beams[3] has made it possible to utilize positrons in surface and near-surface studies. By adjusting the incident beam energy from several eV up to 50 keV, the region from the outermost atomic layers to the depth of several μm can be monitored. Positrons are, due to their positive charge, sensitive to open-volume defects inside the crystal (see, e.g., Ref. 3). The first study of metallic epitaxial overlayers with positrons was performed by Schultz et al.[4] They studied Cu grown on W(110) and were able to observe positron trapping at defects near the interface. Köymen et al.[5] have compared positron results with low-energy-electron-diffraction (LEED) measurements in homoepitaxial Ni(110) structures. Alkali-metal-covered Ni surfaces have been examined in order to study positronium (Ps) formation on a metallic surface.[6] Gidley and Frieze developed[7] the concept of reemitted positron energy spectroscopy (RPS), which has recently been used by Ociepa et al.[8] to study the growth of Co on W(110) in connection with LEED and Auger-electron-spectroscopy (AES) measurements. Gidley[9] has also studied with RPS the phase transition from coherent to incoherent growth when Ni is evaporated on different low-index Cu surfaces.

Positron measurements normally include a lot of information from the region well below the surface. The most surface-sensitive quantities are the branching ratios to different surface channels. They give information on the positron-surface interaction, as well as on other physical phenomena occurring at the surface. In this work we have changed the surface conditions in a controlled manner by evaporating foreign material on a single-crystal substrate. Experiments have been done with positrons, LEED, and AES for Cu grown on Ag(111) and Ag grown on Cu(111). The studied overlayer thicknesses vary, respectively, from 0.1 monolayers (ML) up to 10 ML and from 0.1 ML up to 100 ML. Both systems have been previously studied by using various techniques. When Cu is grown on Ag(111), the growth has been reported to start by formation of either one[10] or two[11,12] complete ML and to proceed by island formation [i.e., the Stranski-Krastanov (SK) growth mode]. In this work we observed the one monolayer to be formed before islanding. In the complementary system, Ag/Cu(111), layer-by-layer growth proceeds beyond the detection limit of Auger-electron spectroscopy[11,13,14] in accordance with our observations. We are not able to correlate the positron results with structural changes in overlayers, but new information on mechanisms governing positron-surface interaction can be extracted.

The rest of the paper is organized as follows. In Sec. II the positron-surface interaction is discussed. Experimental conditions and measured quantities are described in Sec. III. Results are presented in Sec. IV and discussed in Sec. V. The paper is concluded in Sec. VI.

II. POSITRON-SURFACE INTERACTION

All positron measurements presented in this paper are based on the analysis of the positrons that have diffused back to the entrance surface after implantation (see, e.g. Ref. 3). After penetrating the solid keV energies, positrons rapidly lose their energy (< 10 ps) and undergo a diffusive motion at thermal energies. Diffusion is governed by scattering from acoustic phonons (for a review on thermal positron motion, see Ref. 15). During the positron lifetime (~ 100 ps), a certain fraction of them, depending on the incident energy, reenter the surface. The flux of positrons can be evaluated using the

diffusion model (see, e.g., Refs. 3, 16, and 17). In the very thin overlayers presently considered, the positrons stopping into the overlayer can be neglected. The positron backdiffusion probability $J(E)$ for an incident energy E is equal to the Laplace transform of the implantation profile $p(z,E)$ as

$$J(E) = \int_0^\infty p(z,E)\exp(-z/L_+)dz , \qquad (1)$$

where L_+ is the positron diffusion length. For the positron implantation profile we have adopted the form of the Gaussian derivative: $p(z,E) = \{\exp[-(z/z_0)^2]\}dz$ with $z_0 = (4.5 \,\mu\mathrm{g\,cm}^{-2})\,[E/(1\,\mathrm{keV})]^{1.55}.$[18,19]

After thermalization and backdiffusion, those positrons returning to the surface have several possible fates. The most common interaction processes at a metal surface are (i) reemission into the vacuum as a free positron,[20] provided the positron work function is negative; (ii) localization of the positron into the image-induced potential well or trapping into a surface defect;[21] (iii) emission as a positronium (Ps) by a pickup of a near-surface electron;[22] (iv) emission as a Ps atom due to the thermal excitation from a surface bound state;[23] and (v) reflection of the positron wave by the potential at a surface.[24,25]

The positron surface processes have recently been a subject of extensive studies. The understanding of positron-surface interaction was revised to some extent when it was observed that reflection from the surface potential is one of the major positron processes at the surface, especially dominant at lower temperatures.[25,26] Positron energetics plays an important role when surface processes are discussed. Positron emission is mainly an elastic process governed by the positron work function ϕ_+.[27,28] Spontaneous reemission occurs if ϕ_+ is negative. Ps emission, an energetically more favorable process than e^+ emission, is a nonadiabatic process with a sudden pickup of e^- at the low-electron-density tail at the surface and subsequent emission as a Ps atom.[29] Experimentally it has been observed that Ps formation and reemission show a similar temperature dependence on surfaces.[25] This suggests that Ps formation can be relatively accurately described by a two-process model. Positron transmission through the surface potential gives almost all the T dependence, and it can be treated separately from the choice between electron pickup and free positron emission, which is done independent of the temperature. Positron trapping into the surface state happens via electron-hole pair excitation showing only weak temperature dependence.[30] In the present work we have adopted to some extent a different way to study positron-surface interaction. Positron energetics is changed by evaporating a foreign material on a single-crystal substrate. This effects the surface dipole component on the work function.

At the interface of two bulklike materials, a thermal positron experiences a potential difference, which equals the difference of the material specific positron affinities. For a detailed discussion on the interface potential, see Refs. 31 and 32. The magnitude of the positron affinity for Ag is 0.55 eV larger than for Cu.[31] Thus, when Cu is grown on Ag(111), a potential barrier preventing the es-

cape of thermal positrons is formed on the surface. In the complementary case, Ag/Cu(111), thermal positrons gain energy from the interface and rethermalize in the layer or reach the surface with hyperthermal energies.

III. EXPERIMENT

A. Experimental conditions

The experiments were performed with a magnetically guided positron beam in an ultrahigh-vacuum system. The beam has been discussed fully elsewhere.[33] We obtain with a ^{58}Co source and a W(110) backscattering moderator a current of typically $10^6 e^+/\mathrm{s}$ at the sample. The energy of the beam was varied from 0 up to 25 keV in the present work. We achieved the energy width ≤ 3 eV, and the beam diameter was approximately 3 mm at the sample location. The pressure during the measurements was below 5×10^{-10} mbar from which it rose during the in situ evaporations up to 8×10^{-10} mbar. The measurement chamber is equipped with 4-grid retarding-field analyzer for LEED and AES analysis, ion sputtering, and residual-gas-analysis facilities for sample and vacuum characterization. A high-purity Ge detector is utilized to monitor the annihilation γ rays.

Both of the high-purity single-crystal samples [99.999% pure Ag(111) and 99.9999% pure Cu(111)] were mechanically and electrolytically polished prior to the insertion in the vacuum system. The samples were cleaned in situ by Ar$^+$-ion etching, first with a high energy (>1 keV) and finally with a lower energy (250–500 eV). After each sputtering cycle the samples were given a heat treatment at a high temperature [Ag(111) at 700 °C and Cu(111) at 750 °C] for ~30 min in order to anneal out the sputtering-induced damage from the surface. Auger-electron spectroscopy was used to confirm the chemical cleanliness of the crystal surfaces. It showed no trace of carbon and oxygen contamination above the 0.1-ML level. In Cu crystals sulfur is a common bulk impurity, which segregates to the surface.[34] We did not observe any sulfur in our crystals. For checking the crystalline order both LEED and positronium fraction measurements[35,36] were performed.

The evaporations were done with an effusion cell system. Cu and Ag evaporants with a purity better than 99.999% were placed in a crucible made of pyrolythic boron nitride. The crucibles were heated with a standard effusion cell which was efficiently surrounded by cooling water and liquid nitrogen. In addition to cooling, the liquid-nitrogen trap served as a local cryopump which enabled the system pressure to stay near the base pressure during the evaporations. When the Auger signal intensity is plotted versus evaporation time (AST plot), abrupt changes occur in the slope of the Auger intensity at coverages corresponding to complete monolayers.[37] In order to calibrate the layer thicknesses, we utilize these breakpoints at AST plots. When the growth proceeds by island formation the curves are smooth. Because both systems grow at least partly through the layer-by-layer mode [Cu/Ag(111) 1 ML plus islanding and Ag/Cu(111) at least 3 ML], the 1-ML breakpoint gives a reference in both cases (see Figs. 3 and 6). In the AES experiments

the instrument was tuned to produce the best possible signal from the Ag *MNN* transition emitting a 351-eV electron. The thickness calibrations were done using this peak. The Cu *MNN* peak (60 eV) was disturbed due to the high background of the retarding field analyzer at low electron energies. In the same time the quartz crystal thickness monitor was calibrated and was used to check the stability of the material flux from the effusion oven. The evaporation rate (typically 10^{-2} Å/s) proved to be constant over long time periods. At low coverages (i.e. below 10 ML) a relative accuracy of 10% in the layer thickness determination is achieved.

In a typical measurement sequence at the coverage range from 0 up to 5 ML, we grew three subsequent monolayers and measured the annihilation spectra with typically 10 incident energies from each layer, the grid in front of the sample both positively and negatively biased. After this sequence, taking approximately 45 min, the surface was cleaned by Ar^+-ion sputtering and the crystal was annealed. The thicker overlayers (> 5 ML) were grown and characterized one at a time.

B. Measured quantities

A schematic view of the experimental situation is shown in Fig. 1. Our measurements are based on the manipulation of freely reemitted positrons. They can be either turned back to the sample by a positive bias voltage in the retarding grid or taken away from the sample area by a negative bias. In the latter case the positrons are directed by an $\mathbf{E} \times \mathbf{B}$ filter (not shown in Fig. 1) to annihilate outside the detection area of the γ detector. By following the change in the total count rate T the fraction for reemitted positrons can be determined as

$$f_{e^+} = \frac{T^+ - T^-}{T^+} , \qquad (2)$$

Vacuum   Sample
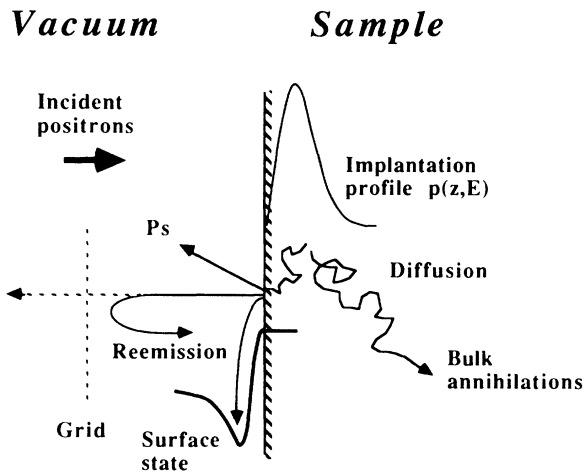
FIG. 1. Schematic view of the experimental arrangement. A fraction of implanted positrons return to the entrance surface where they can escape as a free e^+ or Ps atom, localize into a surface state, or reflect from the surface potential back to the crystal. Reemitted positrons are either turned back to the crystal by a positively biased grid or allowed to escape the detection area by a negatively biased grid.

where T^+ corresponds to the total count rate measured when the grid is positively biased and T^-, respectively, when it is negatively biased.

The positronium emission yield can be determined by distinguishing the 3γ annihilations of the orthopositronium from all other events. In this paper we determined the positronium fraction f by measuring the γ energy spectrum from which f can be calculated using the formula

$$f = 1 \Big/ \left[1 + \frac{P_1}{P_0} \frac{(R_1 - R)}{(R - R_0)} \right] , \qquad (3)$$

where the ratio R is defined by $R = (T - P)/P$. T is the rate of detected γ quanta in the whole energy spectrum and P correspondingly those detected in the 511-keV annihilation peak. The calibration parameters R_1 and R_0 correspond to the situation where 100% and 0% of positrons, respectively, are emitted as positronium atoms from the surface. Their values depend strongly on the measurement geometry.[38,16] Typical values for parameters are $R_1 = 12.0$, $R_0 = 3.5$, and $P_1/P_0 = 0.4$. If we denote the fraction calculated in this way when the grid is positively biased (=conventional positronium fraction) with $f_{Ps}^+(E)$ and for negatively biased grid $f_{Ps}^-(E)$, the *energy-independent* thermal positron branching ratios[39,40] for positron emission (ϵ_{e^+}) and Ps emission (ϵ_{Ps}) and other surface events (ϵ_s), respectively, can be written as

$$\epsilon_{e^+} = \frac{f_{e^+}(E)}{J(E)} = \frac{T^+(E) - T^-(E)}{T^+(E)} \Big/ J(E) , \qquad (4)$$

$$\epsilon_{Ps} = \frac{f_{Ps}(E)}{J(E)} = \frac{f_{Ps}^-(E)[1 - f_{e^+}(E)]}{J(E)} , \qquad (5)$$

and

$$\epsilon_s = 1 - \epsilon_{Ps} - \epsilon_{e^+} , \qquad (6)$$

where f_{Ps} is the true Ps fraction. $J(E)$ is the returning probability for the incident energy E, and it can be calculated as the known positron diffusion length. For the positron diffusion length in Cu we adopted the value $L^+ = 1400$ Å, and for Ag, correspondingly $L^+ = 1100$ Å,[17] which are the values measured from the same crystals used in the present study.

In addition to the branching ratio measurements and positronium fraction measurements, we performed detailed reemission measurements with some incident energies in order to get information on the energy distributions of reemitted positrons. The measurements were done by changing the bias between the sample and the retarding grid and monitoring the total count rate. In this way the integral yield distribution is measured, and by differentiating it the energy distribution of the emitted positrons can be obtained (see, e.g., Ref. 4).

IV. RESULTS

Both the substrate crystals used in this study, Cu(111) and Ag(111), are smooth close-packed fcc surfaces. Copper and silver have a small mutual solubility, and are

the only material pair among the noble metals that does not alloy.[1] We define a monolayer (ML) as to corresponding to the atomic density of the substrate surface, since both systems begin to grow coherently. The atomic densities for Cu(111) and Ag(111) are 4.3×10^{15} and 3.4×10^{15} cm^{-2}, respectively. When Cu grows on Ag(111), the lattice structure is more open than that of Cu(111), favoring the formation of the open-volume defects as the lattice parameter relaxes towards Cu(111) lattice parameters. In the complementary case the Ag overlayer is compressed and it seems less likely that open-volume defects capable to trap positrons are formed. These phenomena have been observed in thick layers and are discussed in a separate publication.[32]

The positron branching ratios for the major escape processes are denoted by ϵ_{e^+} for reemission and ϵ_{Ps} for Ps emission. In the present experimental arrangement it is not possible[26] to distinguish surface localization and reflection back to the bulk from each other. Thus, we are only able to obtain their sum $\epsilon_s = \epsilon_{ss} + \epsilon_{refl}$ [Eq. (5)]. A way of distinguishing surface trapping and reflection would be, e.g., to study the fraction of positrons annihilating at the surface state through the intensity of the surface lifetime component. The three branching ratios were determined for each incident positron energy. An example is shown in Fig. 2, where data from the 17 ML Ag/Cu(111) structure is shown. From Fig. 2 it can easily be seen that the branching ratios vary in the low-energy region. This is due to nonthermal effects,[41] where positrons escape from the crystal before completion of thermalization (see Sec. V). The branching ratios were determined by taking the arithmetic average of the values corresponding to incident positron energies between 4 and 12 keV. The upper-limit energy value is determined
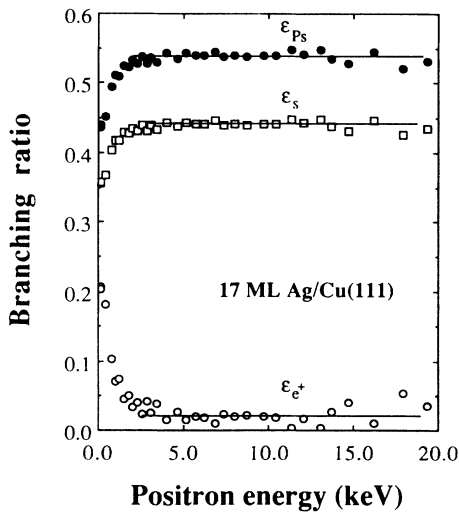
by the decrease in the backdiffusion probability, which decreases the signal and thus increases the statistical uncertainty.

A. Cu/Ag(111)

The LEED pattern was monitored around an electron energy of 150 eV as the Cu growth proceeded. The pattern remained a sharp $p(1 \times 1)$ up to 0.5 ML. Only a slight increase in the spot intensity when compared to the background signal was observed. Above 0.5 ML the LEED pattern was still $p(1 \times 1)$ showing, however, clear tails in spots. This indicates that Cu growth on Ag(111) begins at submonolayer coverages by the formation of two-dimensional islands due to net attractive Cu-Cu lateral interactions. Above 1 ML, a sharp decrease in the ratio between beam and background intensities was observed supporting the AST observation (Fig. 3) about three-dimensional islanding after 1-ML completion. The dashed line in Fig. 3 corresponds to layer-by-layer growth calculated based on the semiempirical curve of Seah and Dench for the inelastic mean free path (IMFP) of electrons.[42] From our data we obtain an IMPF of 13.3 Å for 351-eV electrons in Cu, which agrees well with the semiempirical value for the IMFP of 10.3 Å.

In Fig. 4, the branching ratios measured as a function of an epitaxial Cu coverage on Ag(111) are presented. In this case the reverse interface potential [theoretically $\Delta \chi_+ = 0.55$ eV (Ref. 31)] prevents the escape of those thermalized positrons implanted into the substrate to the surface. The work function ϕ_+ of Ag(111) for a positron is positive and during the Cu ($\phi_+ = -0.3$ eV at room temperature[43]) growth the energy level of thermal positrons in Ag never exceeds the vacuum level. These facts close the reemission as an escape channel throughout the coverage range. Being energetically allowed Ps formation is possible from Ag(111) with a probability of 0.4 at room temperature. The abrupt decrease in the Ps forma-

FIG. 2. Experimental branching ratios ϵ_{e^+}, ϵ_{Ps}, and ϵ_s of positron to various surface interface channels as a function of incident positron energy measured from 17-ML Ag on Cu(111). The variable behavior below 2 keV is due to nonthermal effects (Ref. 41), and the constant level at $E > 2$ keV describes thermal e^+ branching ratios into channels.
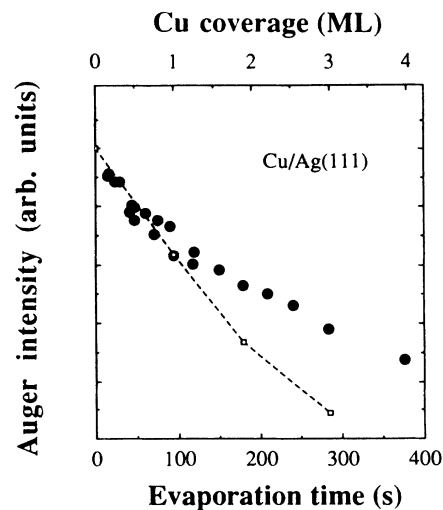
FIG. 3. Auger signal vs evaporation time (AST) plot for the Cu/Ag(111) system. The dashed line corresponds to layer-by-layer growth predicted by the semiempirical formula of Seah and Dench (Ref. 42). Squares denote the completion of a monolayer.
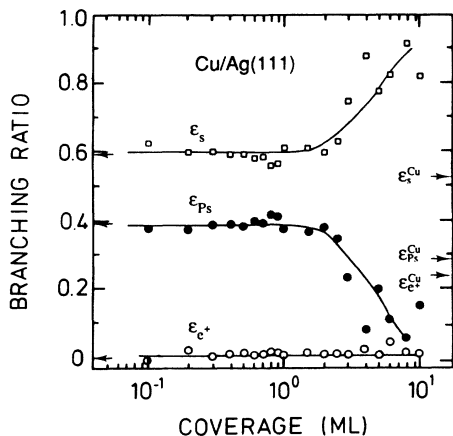
FIG. 4. Thermal positron branching ratios ϵ_{e^+}, ϵ_{Ps}, and ϵ_{ss} as a function of Cu coverage on Ag(111). Solid lines are guides for the eye. The arrows on the left and right are for clean Ag(111) and Cu(111), respectively.

FIG. 5. Integral distributions of reemitted positron yield vs grid-bias voltage measured from 40-ML Cu/Ag(111), bulk Cu(111), and 4-ML Cu/Ag(111) at incident positron energy 500 eV. The data measured from Ag(111) coincide with those from 4-ML Cu/Ag(111).

tion between 2 and 3 ML can again be attributed to the formation of the interface potential. In this coverage region the positron wave still has some overlap with the low-electron-density tail outside the surface, where Ps formation occurs. The simultaneous increase in ϵ_s, which actually is a complement to the sum of ϵ_{e^+} and ϵ_{Ps}, reflects the same phenomenon. The arrows in the figure correspond to the branching ratios for bulk Ag(111) and Cu(111) (see also Table I). The branching ratio curves do not approach the bulk values for Cu(111) due to the reverse positron potential, which prevents thermal positrons from reaching the surface, making the analysis impossible.

The measured integral distributions of reemitted positrons from 4-ML .Cu/Ag(111), 40-ML Cu/Ag(111), and Cu(111) for the incident energy 500 eV are shown in Fig. 5. The distribution from Ag(111) coincides with 4-ML Cu/Ag(111), and no thermal emission is observed due to the positive work function. The total yield of 5% observed from 4-ML Cu/Ag(111) arises totally from a nonthermal contribution. The total yield of 40-ML Cu/Ag(111) has not reached the level of Cu(111). There are two reasons for that. A fraction of the positrons is implanted beyond the interface and slows down to energies where it cannot overcome the reverse interface barrier. On the other hand, open-volume defects in the overlayer may reduce the amount of returning positrons through trapping.

B. Ag/Cu(111)

The growth observed when Ag is evaporated on Cu(111) is much more ordered than in the complementary case. The AST analysis (Fig. 6) shows that the layer-by-layer growth mode continues for at least 2, maybe 3, ML, which is supported by LEED patterns showing relatively sharp spots and a low background up to 5 ML. The dashed lines in Fig. 6 correspond again to layer-by-layer growth. The Ag Auger intensity follows the predicted curve giving an IMFP corresponding well to that calculated from the semiempirical formula.[42] The intensity for bulk Ag was taken from that corresponding to

TABLE I. Thermal positron branching ratios for pure defect-free Cu(111) and Ag(111) surfaces at 300 K.

	Cu(111)	Ag(111)
ϵ_{Ps}	0.29	0.40
ϵ_{e^+}	0.23	0.01
ϵ_s	0.48	0.59
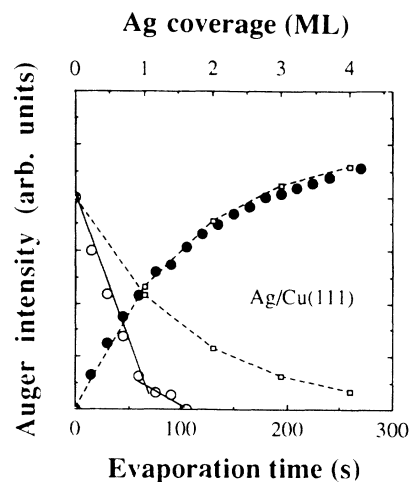
FIG. 6. Experimental Auger signal vs evaporation time (AST) plot for the Ag/Cu(111) system. Solid dots correspond to the Ag MNN transition and the open ones to the Cu MNN transition. Dashed lines with open squares at each completion of a monolayer correspond to layer-by-layer growth predicted by the semiempirical formula of Seah and Dench (Ref. 42). The solid line is a guide for the eye.
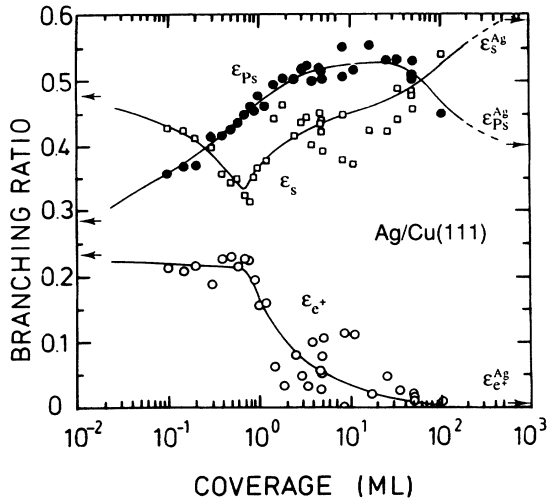
FIG. 7. Experimental branching ratios ϵ_{e^+}, ϵ_{Ps}, and ϵ_{ss} as a function of Ag coverage on Cu(111). Solid lines are guides for the eye. The arrows on the left and right are for clean Cu(111) and Ag(111), respectively.

FIG. 8. Integral distributions of reemitted positron yield vs grid-bias voltage measured at 4-ML Ag/Cu(111), bulk Cu(111), and 40-ML Ag/Cu(111) with incident positron energy 500 eV. The data from Ag(111) coincide with those from 40-ML Ag/Cu(111).

15-min evaporation (~12 ML). The agreement between the predicted and the measured Cu peak attenuations is not so good. The difference can be attributed to the low sensitivity of the used retarding-field analyzer at low electron energies. From Cu data we obtain an IMFP 1.6 Å for 60-eV electrons in Ag, which is much smaller than the predicted 3.8 Å. However, the Cu data also show a clear breakpoint at approximately a 1-ML coverage (solid line in Fig. 6).

The branching ratios for the system Ag/Cu(111) are shown in Fig. 7. Several interesting features can be observed in the curves. The simplest of the positron surface processes is (quasi)elastic positron reemission. Its probability decreases only slightly at submonolayer coverages until, after the completion of the first overlayer, it starts to decrease rapidly. Above 10-ML coverage there is no reemission, due to the positive work function of silver. Between 2 and 10 ML the data are scattered. The reasons for this will be discussed later. The Ps-formation probability begins to increase from the very beginning (>0.1 ML) and continues to do so up to 5 ML. After this thickness the ϵ_{Ps} curve begins to approach the value corresponding to bulk Ag. From the ϵ_s curve we observe that below 1 ML the fraction of positrons remaining in the bulk or trapping into the surface state is reduced strongly. Above 1 ML the rise starts towards the bulk value. The arrows in the figure correspond to bulk Cu(111) and Ag(111) (see Table I).

In Fig. 8 the integral distribution of reemitted positrons is shown measured with 500-eV incident positron energy for 4-ML Ag/Cu(111) together with those for 40-ML Ag/Cu(111) and Cu(111) for comparison. Ag(111) distribution is equal to that of 40-ML Ag/Cu(111). 4-ML Ag/Cu(111) is in the coverage region in which the branching ratio measurements show scattered data (Fig. 7). From Fig. 8 we can conclude that the 4-ML Ag/Cu(111) structure shows, in addition to nonthermal
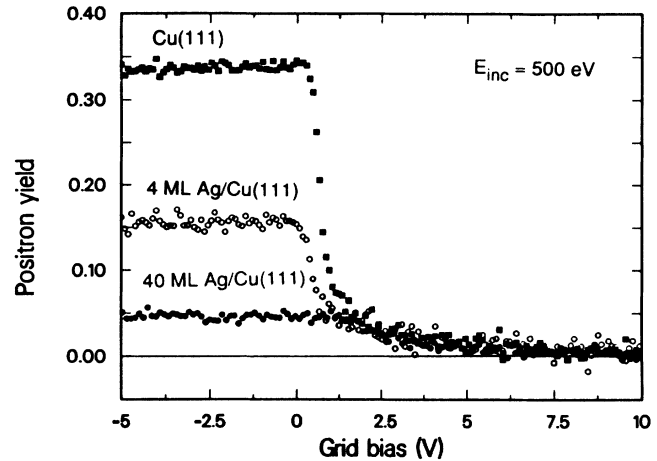
positrons, a remarkable component of thermal positrons. The distribution is slightly broadened when compared to clean Cu(111) and its center of mass is moved towards positive work-function values.
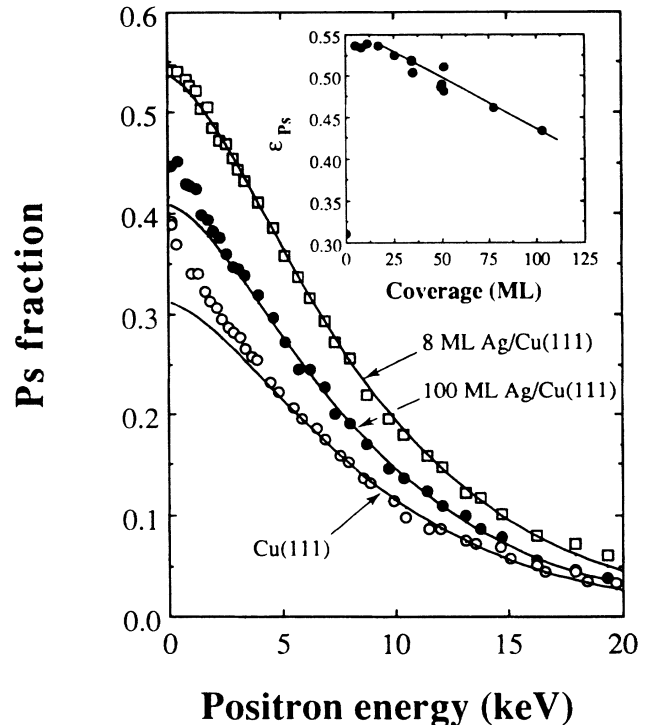
FIG. 9. Experimental Ps fractions vs incident positron energy from bulk Cu(111) (open dots), from the 8-ML Ag/Cu(111) structure (open squares), and from the 100-ML Ag/Cu(111) structure (solid dots). Solid lines correspond to the best least-squares fits with fixed diffusion length $L_+ = 1400$ Å. The inset shows the branching ratio for the Ps emission in an expanded scale (see Fig. 7).

The results of the positronium fraction versus incident positron energy for three different samples are presented in Fig. 9. The lowermost of the measured data sets (open dots) originates from defect-free bulk Cu(111). In the center (solid dots) data obtained for 100-ML Ag/Cu(111) are shown and the uppermost data set (open squares) corresponds to an 8-ML Ag/Cu(111) structure. The thinner overlayer is thin enough so that positron stopping in it can be neglected, and the curves describe positron diffusion in the Cu substrate, whereas in the 100-ML structure positrons start to thermalize at low incident energies (<2 keV) within the overlayer. We have applied the standard diffusion model for the semi-infinite crystal for the data. The solid lines in Fig. 9 present the best least-squares fits with a fixed positron diffusion length for Cu $L_+ = 1400$ Å.[17] It can be observed that the diffusion model explains the data obtained for the 8-ML Ag/Cu(111) structure throughout the entire energy range, whereas in the other two curves it was necessary to omit the low-energy data points, which have a considerable contribution from epithermal positrons. In the 100-ML Ag/Cu(111) case, skipping of data points below 4 keV was necessary before the diffusion analysis was capable of modeling the data. For Cu(111) the minimum energy is $E_{min} = 6$ keV.[17] In the inset of Fig. 9 the branching ratio for Ps emission is shown as a function of Ag coverage in a linear coverage scale and expanded ϵ_{Ps} scale. The data are the same as shown in Fig. 7 in the logarithmic coverage scale. A linear decrease is observed in the Ps-emission probability as the Ag layer thickens on Cu(111).

V. DISCUSSION

A. Comparison with earlier experiments

Several studies exist on the early stages of epitaxial growth of Cu on Ag(111). Horng and Vook[44] report the Stranski-Krastanov (SK) growth mode at room temperature. 2 ML are formed prior to island formation, whereas the growth on a substrate at 500 K shows three-dimensional islands from the very beginning. Gibson and Dobson[10] have done similar observations with 1-ML SK growth at 300 K. Recently, the Cu/Ag(111) system has been studied with surface extended energy-loss fine-structure (SEELFS) (Ref. 12) and extended fine Auger structure (EXFAS) (Ref. 45) measurements. In these experiments it is observed that Cu growth begins commensurately but the registry breaks down between the third and fifth layers. Shapiro et al.[13] report surface segregation of Ag even at room temperature. If we combine these, to some extent controversial results, with our observations of 1-ML SK growth, no unique conclusions can be done. The differences are probably due to slight differences in sample preparation. The Cu/Ag(111) structures seem to be very unstable and Ag readily enriches to the surface: a 5 min/200 °C heat treatment to 40-ML Cu/Ag(111) leads to an observation of a clear Ag signal by AES.

Ag/Cu(111) has been an attractive system for studying two-dimensional electronic structure in overlayers.[46,14] The layer-by-layer growth and the sharp interface allow

such studies. Early experiments showed island growth,[47] whereas in recent experiments it has been shown convincingly that the growth proceeds layer by layer at least to 2 ML.[11,14] These are in good accordance with our AST results suggesting at least 3 complete monolayers be formed. Shapiro et al.[46] have observed the monolayer formation to appear via large monolayer thick islands incommensurately with the substrate. The overlayer and the substrate are growing mutually parallel, i.e., they have the same crystal orientation. Our observations do not support incommensurate growth.

B. Positron surface processes

In the present work we have followed the positron-surface interaction by changing the positron energetics at the surface with adsorbates. The situation is different from temperature-controlled experiments, in which the temperature influences mostly the bulk energetics.[26] In the present study adsorbates at submonolayer coverages change directly the surface dipole making the understanding of surface processes more complicated. The influence of the energy-level changes can most directly be observed from ϵ_{e^+} curves in Figs. 4 and 7. In Fig. 4 the negligible reemission probability throughout the coverage range reflects two facts: Firstly, it manifests the positive work function for Ag(111), and secondly the existence of the reverse potential barrier, which is formed when Cu is grown on Ag(111). When Ag is grown on Cu(111), the effect of an interface potential can also be observed. According to calculations, the difference between the positron affinities (i.e., the interface potential height) in Cu and Ag is $\Delta\chi_+ = 0.55$ eV (Ref. 31) and the Ag(111) work function $\phi_+^{Ag} = 0.62$ eV.[48] This means that a thermal positron must overcome a potential barrier of 0.07 eV in order to be able to escape as a free positron if the Ag overlayer has the properties corresponding to the bulk Ag. Secondary effects (e.g., in sample preparation) can cause shifts of 0.1 eV in energy levels, and thus the scatter in the data between 2 and 10 ML is interpreted to be due to this phenomenon. This is supported by the 4-ML Ag/Cu(111) integral distribution in Fig. 8, in which a clear contribution from positrons emitted from the substrate can be observed. Above 10 ML, the interface is fully formed and free positrons cannot escape through the Ag(111) overlayer. The nonzero branching ratio for reemission from Ag(111) (see Table I) indicates that the work function for Ag(111) is relatively near the vacuum level, and positrons at the tail part of the Maxwell-Boltzmann energy distribution may be able to escape as free positrons.

In principle, there are two main factors influencing the distribution of emitted Ps atoms: the initial combined positron-electron state at the surface and the Ps-formation mechanism. The Ps emission probability is proportional to the expression[29,49]

$$\epsilon_{Ps} \propto \int_p d\mathbf{p} \sum_j |M_{if}|^2 n_j \delta \left[\frac{p^2}{4m} + E_F - E_j + \phi_{Ps} \right] , \quad (7)$$

where $\mathbf{p}$ is the momentum of the Ps center of mass, E_F is the Fermi energy, n_j and E_j are the occupation number

THIN Cu/Ag(111) AND Ag/Cu(111) STRUCTURES . . .

and energy of the jth electron state, and m is the electron mass. M_{if} is the matrix element giving the coupling between initial and final combined electron-positron states. In the case of thin layered structures, where the interface potential is fully developed and rethermalization in the overlayer plays a minor role, the positronium formation potential ϕ_{Ps} can be written

$$\phi_{Ps} = \phi_+ + \phi_- - E_B + \Delta\chi_+ , \qquad (8)$$

where ϕ_+ and ϕ_- are the positron and electron work functions, respectively, the Ps binding energy $E_B = 6.8$ eV, and $\Delta\chi_+$ is the positron affinity difference. We can distinguish two energy-dependent contributions from Eq. (8). By adjusting the positron kinetic energy, the size of the occupied phase space can be controlled, i.e., with increased kinetic energy, positrons may help deeper-bound electrons over the surface barrier by forming a Ps atom with them. On the other hand, the matrix element M_{if} also has an intrinsic energy dependence.

An interesting feature is observed in positron branching of Ag/Cu(111) in Fig. 7 below the 1-ML level. The probability ϵ_s that positrons cannot escape out of the crystal decreases sharply. At the same time the reemission probability stays constant and Ps formation is increased. The Ps formation probability increases already during the formation of the first 0.1 ML from 0.28 to 0.35. This kind of huge change can hardly be accompanied by structural changes in the overlayer or changes in the transmission through the positron potential, because the reemission probability is constant or even slightly decreasing. Adatoms may deform the surface potential and decrease the surface-state trapping probability. Another possible explanation is the enhanced electron density at the surface making positronium formation more likely. 2D-ACAR or Ps time-of-flight measurements (see, e.g., Ref. 3) from submonolayer overlayers would provide new insight into these questions. A similar increase in Ps emission at submonolayer coverages was observed by Gidley et al.[6] when alkali metals were grown on Ni.

Above 1 ML the reemission branch begins to close. The positrons are divided between Ps formation, reflection, and surface-state trapping. Ps formation reaches a constant level at approximately 5 ML, which corresponds to the thickness at which the Ag surface begins to exhibit electronic structure of bulklike Ag(111).[13] The level that the Ps-formation probability reaches is well above that for Ag(111). Hence the change can no longer be attributed to the local changes in the surface potential nor to the electronic-structure changes at the surface. The positron distribution reaching the surface at a 5-ML structure is subject to an energy offset equal to the positron affinity difference between Ag and Cu. Rethermalization can still be neglected. Thus, positrons encounter the Ag(111) surface having approximately 0.5 eV higher energy than in the semi-infinite case. The difference in the Ps formation probability can hardly be associated with the decreased surface-state trapping rate, which instead should be even slightly increased as the positron energy is increased.[30] The effect of reflection is considered to be minor, because the dominating feature

in the reflection seems to be due to the image tail of the surface potential.[26] This leaves only the Ps emission process itself as a possible explanation to the increase. The energy excess $\Delta\chi_+$ [Eq. (9)] makes it possible that epithermal positrons can pick up electrons deeper below the Fermi level than thermal positrons from semi-infinite Ag(111), and help them into the vacuum by forming a Ps atom. This increases the total probability of Ps emission. However, the energy dependence of the matrix element M_{if} in Eq. (8) must also be considered as one candidate to the increase. Above 10 ML, rethermalization in the overlayer[50] starts to play a role and the branching characteristics approach those corresponding thermal positrons on Ag(111) (see inset of Fig. 9).

Summarizing, the observed changes in Ps emisson in Ag/Cu(111) cannot be accounted for from a single process, and at least two phenomena increasing the Ps emission are required. Furthermore, coupling between different surface processes is not yet unambiguously understood. Further experiments and theoretical developments are needed in order to explain these phenomena completely.

C. Crystal growth at the submonolayer level with positrons

One of the objectives of the present work was to study the feasibility of the positrons in observing defects in the early stages of crystal growth. At submonolayer coverages the surface contains a lot of potential positron traps (i.e., surface vacancies). Köymen et al.[5] have reported positronium fraction measurements from homoepitaxy on a Ni(110) surface. They were able to observe positron trapping at submonolayer coverage and relate this to the ledge density in the outermost surface layer. We did not observe this kind of behavior either at our bimetallic structures or at approximately 1-ML-thick Cu/Cu(111) structures. This is demonstrated in Figs. 4 and 7 for bimetallic structures. The branching ratios measured for the systems Cu/Ag(111) (Fig. 4) and Ag/Cu(111) (Fig. 7) do not show any trapping behavior below 1 ML. On the contrary, the escape probability in Ag/Cu(111) has even increased. The reason for this is that the possible positron trapping is damped out by the changes in the positron energetics or by the changes in the electron density at the surface. These phenomena are so strong that changes induced by them in the branching ratios dominate the features in Figs. 4 and 7 below 1 ML, as discussed above. On the other hand, measurements for homoepitaxial Cu structures gave results corresponding to bulk Cu, i.e., no signs of positron trapping into surface defects were observed.

D. Epithermal effects in diffusion analysis

There has been an intense recent discussion concerning epithermal positrons. They are observed at low incident energies when either Ps formation or reemission probabilities are monitored as a function of incident positron energy. The fraction of emitted Ps or e^+ has generally been larger than predicted by the diffusion model at incident positron energies of a few keV. The measured signal is, according to the diffusion model, proportional to the

product of the backdiffusion probability and the branching ratio either to the positron or Ps. So far these effects have been attributed totally to the abnormally high return probability of positrons due to the faster transport of nonthermal positrons,[51] and deviations in the positron implantation profile from the standard behavior at higher E_{inc}. However, our experiments indicate the surface branching ratios to be dominantly responsible for most of the discrepancy from the diffusion model.

The diffusion model can be used in analyzing data from bulk samples, if data measured with low incident energies are omitted.[16] For Cu(111) this skipping energy minimum is $E_{min} = 6$ keV and for Ag(111) it is $E_{min} = 3$ keV.[17] In bilayered structures with the interface potential allowing escape from the substrate, the diffusion model may be applied with the same considerations as in the bulk samples, if the positron stopping into the overlayer can be neglected. The diffusion coefficient corresponding to the substrate is then obtained. When the implantation into the overlayer is significant, the interface potential constrains positron motion, which can be included into the diffusion model via boundary conditions.[32]

In Fig. 9 it is observed that $f_+(E)$ data from Cu(111) as well as from 100-ML Ag/Cu(111) structure show characteristic features of data measured from bulk samples. The Ps fraction is increased from that predicted by the diffusion model at low incident energies. The majority of the positrons return with thermal energies, and the epithermal positrons are a minor part of the population. However, the epithermal contribution is overemphasized in the measured signal due to a much higher transmission probability through the surface potential, leading to strongly-energy-dependent branching ratios.

When the results from thin (5–20-ML) Ag/Cu(111) structures were analyzed, it was observed that $f_+(E)$ data can be modeled using the diffusion model throughout the incident energy scale from 0.5 up to 25 keV. Positrons have obtained at the interface an energy excess relative to the positron ground state at Ag, which is much larger than the positron thermal energy. At low coverages, positrons have a high probability of returning to the surface without energy losses, and hence almost all positrons interact with the surface at epithermal kinetic energies having weakly-energy-dependent branching ratios. Above 20 ML, rethermalization in the overlayer becomes significant, leading again to bulklike behavior of the Ps fraction. A small fraction of positrons having kinetic energy above the vacuum level is able to escape as free positrons below 2-keV incident energy (Fig. 2). On the other hand, Ps emission is possible for the whole positron population, and it is evident that the obtained energy excess is responsible for the validity of the diffusion model.

Therefore we are emphasizing the importance of the energy dependence of the branching ratios. Our observations suggest that the fraction of positrons approaching the surface is proportional to the Laplacian of the implantation profile according to Eq. (1), with incident energies above 0.5 keV. Furthermore, positron implantation profile of the Gaussian derivative shape is adequate to de-scribe positron stopping as $E_{inc} > 0.5$ keV. Positron motion inside the solid can be described within the diffusion model obeyed by both thermal and epithermal positrons over a wide energy range. The observed discrepancy with the diffusion model is due to the energy dependence of positron transition rates to different surface processes.

VI. SUMMARY

In this study we have examined positron behavior in thin epitaxial overlayers. Measurements have been done from (0.1–10)-ML-thick Cu layers on Ag(111) and (0.1–100)-ML-thick Ag/Cu(111) structures. We have studied thermalized positron surface processes as a function of coverage and incident positron energy. Reemission measurements have also been performed to get information on positron energy distribution and thermalization. The growth has also been characterized by LEED and AES.

When Cu is grown on Ag(111), the growth is observed to begin by the formation of one complete monolayer. After this the growth proceeds via three-dimensional island formation. Positron behavior is dominated by the formation of a reverse interface potential which prevents the escape of thermal positrons from the crystal. Ag/Cu(111) grows in better registry than the complementary system. The growth characteristics show layer-by-layer growth for at least 3 ML. Again, changes in positron energy levels induce the dominant features in the measured signals. An enhanced Ps formation probability even below 0.1-ML coverage indicates a drastic change in the positron surface potential or the electron density of states at the surface. In thicker overlayers the increased positron kinetic energy further increases the Ps emission probability. We emphasize that we observe no signs of positron trapping at defects during the crystal growth due to the dominant role of surface and interface potentials. It is evident that differences in positron affinities in bimetallic structures limit the applicability of the method to detect open-volume defects near the interface unlike in the case of a semi-infinite homogeneous sample.[35,36] These subjects, however, need further experimental and theoretical work.

Positron fraction versus incident positron energy measurements suggest a new interpretation of epithermal phenomena occurring in these experiments. Up to now they have been attributed to the deviation in the implantation profile at low energies resulting in an increased returning probability, and a significant contribution of positrons returning to the surface prior to the thermalization. Our observations indicate that the commonly accepted positron implantation profile at higher positron energies is also valid down to 0.5 keV. Furthermore, thermal and epithermal positrons can roughly be described with the same diffusion constant. The key property leading to an enhanced e^+ and Ps emission is the energy dependence of the positron branching ratios, rather than deviations in positron current approaching the surface. The sharpening in the Ps fraction data is thus mainly due to the enhanced transmission probability of nonthermal positrons through the surface potential.

ACKNOWLEDGMENTS

*Present address: Outokumpu Electronics, P.O. Box 85, SF-02201, Espoo, Finland.

†Present address: Outokumpu Group, P.O. Box 280, SF-00101, Helsinki, Finland.

[1] E. Bauer, in *The Chemical Physics of Solid Surfaces and Heterogeneous Catalysis,* edited by D. A. King and D. Woodruff (Elsevier, Amsterdam, 1984), Vol. 3B.

[2] See, e.g. *Solid State Physics: Surfaces,* Vol. 22 of *Methods of Experimental Physics,* edited by R. L. Park and M. G. Lagally (Academic, New York, 1985).

[3] P. J. Schultz and K. G. Lynn, Rev. Mod. Phys. **60**, 701 (1988).

[4] P. J. Schultz, K. G. Lynn, W. E. Frieze, and A. Vehanen, Phys. Rev. B **27**, 6626 (1983).

[5] A. R. Köymen, D. W. Gidley, and T. W. Capehart, Phys. Rev. B **35**, 1034 (1987).

[6] D. W. Gidley, A. R. Köymen, and T. W. Capehart, Phys. Rev. B **37**, 2465 (1988).

[7] D. W. Gidley and W. E. Frieze, Phys. Rev. Lett. **60**, 1193 (1988).

[8] J. G. Ociepa, P. J. Schultz, K. Griffiths, and P. R. Norton (unpublished).

[9] D. W. Gidley, Phys. Rev. Lett. **62**, 811 (1989).

[10] M. J. Gibson and P. J. Dobson, J. Phys. F **5**, 864 (1975).

[11] E. Bauer, Appl. Surf. Sci. **11/12**, 479 (1982).

[12] T. Tyliszczak, A. P. Hitchcock, and M. DeCrescenzi, Phys. Rev. B **38**, 5768 (1988).

[13] A. P. Shapiro, A. L. Wachs, and T.-C. Chiang, Solid State Commun. **58**, 121 (1986).

[14] Y. Borensztein, Europhys. Lett. **4**, 723 (1987).

[15] T. McMullen, in *Positron Annihilation, Proceedings of the 7th International Conference on Positron Annihilation, New Delhi, 1985,* edited by P. C. Jain, R. M. Singru, and K. P. Gopinathan (World Scientific, Singapore, 1985), p.657.

[16] H. Huomo, E. Soininen, and A. Vehanen, Appl. Phys. A **49**, 647 (1989).

[17] E. Soininen, H. Huomo, P. A. Huttunen, J. Mäkinen, A. Vehanen, and P. Hautojärvi, Phys. Rev. B **41**, 6227 (1990).

[18] S. Valkealahti and R. M. Nieminen, Appl. Phys. A **35**, 51 (1984).

[19] A. Vehanen, K. Saarinen, P. Hautojärvi, and H. Huomo, Phys. Rev. B **35**, 8252 (1987).

[20] A. P. Mills, Jr., P. M. Platzmann, and B. L. Brown, Phys. Rev. Lett. **41**, 1076 (1978).

[21] C. H. Hodges and M. J. Stott, Solid State Commun. **12**, 1153 (1973).

[22] K. F. Canter, A. P. Mills, Jr., and S. Berko, Phys. Rev. Lett. **33**, 7 (1974).

[23] K. G. Lynn, Phys. Rev. Lett. **43**, 391 (1979).

[24] R. M. Nieminen and J. Oliva, Phys. Rev. B **22**, 2226 (1980).

[25] D. T. Britton, P. A. Huttunen, J. Mäkinen, E. Soininen, and A. Vehanen, Phys. Rev. Lett. **62**, 2413 (1989).

[26] P. A. Huttunen, J. Mäkinen, D. T. Britton, E. Soininen, and A. Vehanen, Phys. Rev. B **42**, 1560 (1990).

[27] C. A. Murray and A. P. Mills, Jr., Solid State Commun. **34**, 789 (1980).

[28] E. M. Gullikson, A. P. Mills, Jr., W. S. Crane, and B. L. Brown, Phys. Rev. B **32**, 5484 (1985).

[29] A. P. Mills, Jr., L. Pfeiffer, and P. M. Platzman, Phys. Rev. Lett. **51**, 1085 (1983).

[30] Y. Kong, R. M. Nieminen, P. A. Huttunen, A. Vehanen, and J. Mäkinen (unpublished).

[31] M. J. Puska, P. Lanki, and R. M. Nieminen, J. Phys. Condens. Matter **1**, 6081 (1989).

[32] P. A. Huttunen, J. Mäkinen, and A. Vehanen, Phys. Rev. B **41**, 8062 (1990).

[33] J. Lahtinen, A. Vehanen, H. Huomo, J. Mäkinen, P. Huttunen, K. Rytsölä, M. Bentzon, and P. Hautojärvi, Nucl. Instrum. Methods B **17**, 73 (1986).

[34] R. G. Musket, W. McLean, C. A. Colmenares, D. M. Makowiecki, and W. J. Siekhaus, Appl. Surf. Sci. **10**, 143 (1982).

[35] J. Mäkinen, A. Vehanen, P. Hautojärvi, H. Huomo, J. Lahtinen, R. M. Nieminen, and S. Valkealahti, Surf. Sci. **175**, 385 (1986).

[36] M. D. Bentzon, H. Huomo, A. Vehanen, P. Hautojärvi, J. Lahtinen, and M. Hautala, J. Phys. F **17**, 1477 (1987).

[37] D. C. Jackson, T. E. Gallon, and A. Chambers, Surf. Sci. **36**, 381 (1973).

[38] P. J. Schultz, K. G. Lynn, and H. H. Jorch, in *Proceedings of the International Workshop on Slow Positrons in Surface Science, Pajulahti, 1984,* edited by A. Vehanen (Helsinki University of Technology, Helsinki, 1984).

[39] H. Schut, A. vanVeen, B. Nielsen, and K. G. Lynn (unpublished).

[40] J. Baker, M. Touat, and P. Coleman, J. Phys. C **22**, 4713 (1988).

[41] H. Huomo, A. Vehanen, M. D. Bentzon, and P. Hautojärvi, Phys. Rev. B **35**, 8252 (1987).

[42] M. P. Seah and W. A. Dench, Surf. Interf. Anal. **1**, 2 (1979).

[43] D. A. Fischer, K. G. Lynn, and D. W. Gidley, Phys. Rev. B **33**, 4479 (1986).

[44] C. T. Horng and R. W. Vook, J. Vac. Sci. Technol. **11**, 140 (1974).

[45] T. Tyliszczak, A. P. Hitchcock, and M. DeCrescenzi, Phys. Rev. B **38**, 5768 (1988).

[46] A. P. Shapiro, T. C. Hsieh, A. L. Wachs, T. Miller, and T.-C. Chiang, Phys. Rev. B **38**, 7394 (1988).

[47] R. W. Vook, C. T. Horng, and J. E. Macur, J. Cryst. Growth **31**, 353 (1975).

[48] O. V. Boev, M. J. Puska, and R. M. Nieminen, Phys. Rev. B **36**, 7786 (1987).

[49] A. Walker and R. M. Nieminen, J. Phys. F **16**, L295 (1986).

[50] P. A. Huttunen, A. Vehanen, and R. M. Nieminen, Phys. Rev. B **40**, 11 923 (1990).

[51] H. Huomo, A. Vehanen, M. D. Bentzon, and P. Hautojärvi, Phys. Rev. B **22**, 8252 (1987).